NASA CR 167920

THREE-DIMENSIONAL FLOW MEASUREMENTS IN A TURBINE SCROLL

BY

W. TABAKOFF, B.V.R. VITTAL AND B. WOOD

Supported by:

NATIONAL AERONAUTICS AND SPACE ADMINISTRATION

Lewis Research Center

Grant No. NAG3-26

NASA CR 167920

THREE-DIMENSIONAL FLOW MEASUREMENTS IN A TURBINE SCROLL

by

W. Tabakoff, B.V.R. Vittal and B. Wood

Department of Aerospace Engineering and Applied Mechanics
University of Cincinnati
Cincinnati, Ohio 45221

Supported by:

NATIONAL AERONAUTICS AND SPACE ADMINISTRATION

Lewis Research Center

Grant No. NAG3-26

TABLE OF CONTENTS

	Page
INTRODUCTION	1
RESEARCH SCROLL FACILITY	3
Experimental Investigation	4
Scroll Geometry	5
Instrumentation	5
Probe Mount and Flow Measurement	6
Procedure	6
RESULTS AND DISCUSSION	7
REFERENCES	11
NOMENCLATURE	12
APPENDIX A	14
APPENDIX B	20
FIGURES	26

LIST OF FIGURES

Figure		Page
1	Schematic Diagram of the Experimental Set-Up . . .	26
2	Scroll Schematic Diagram	27
3	Plan View of the Scroll	28
4	Schematic Diagram of the Hot Film Sensor	29
5a	Angular Position of Probe Ports (Section 1) . . .	30
5b	Angular Position of Probe Ports (Section 2) . . .	31
5c	Angular Position of Probe Ports (Section 3) . . .	32
6	Relative Position of Three Sections with Respect to the Machine Axis	33
7	The Inlet Velocity Distribution	34
8a	Normalized Through Flow Velocity Contours (Section 1)	35
8b	Normalized Through Flow Velocity Contours (Section 2)	36
8c	Normalized Through Flow Velocity Contours (Section 3)	37
9	Secondary Flow Velocity Vectors (Section 1) . . .	38
10	Schematic Diagram of Recirculation Zones (Section 1)	39
11	Horizontal Components of Secondary Flow Velocity Vectors (Section 1)	40
12	Secondary Flow Velocity Vectors (Section 2) . . .	41
13	Schematic Diagram of Recirculation Zones (Section 2)	42
14	Horizontal Components of Secondary Flow Velocity Vectors (Section 2)	43
15	Secondary Flow Velocity Vectors (Section 3) . . .	44
16	Schematic Diagram Showing Recirculation Zones (Section 3)	45

Figure		Page
17	Horizontal Components of Secondary Flow Velocity Vectors (Section 3)	46
18	Probe Coordinate Axes	47
19	Probe Measurement Positions and Nomenclature, Viewed from Above Along Probe Axis	48

SUMMARY

A study was conducted to determine experimentally the flow behavior in combined scroll nozzle assembly of a radial inflow turbine. Hot film anemometry technique was used to measure the three dimensional flow velocity in the scroll. The through flow and secondary flow velocity components are measured at various points in three scroll sections.

INTRODUCTION

In recent years there has been considerable interest in the study of small radial gas turbines in order to improve their performance characteristics. Most of the research work has been concentrated on turbine rotors, since they were considered to have the most significant effect on turbine efficiency. Recently, research work has demonstrated a need for new design techniques in the turbine scroll and guide vanes.

At the present time the scroll designs are still based on one dimensional flow calcul .tions. Guide vane blades are merely designed to give the required flow turning angle. The inlet velocity distribution is assumed to be uniform from one guide vane inlet to another. Such an assumption is not realistic; a variation in the inlet velocity distribution exists and depends mainly on the scroll and the guide vane blade effects. Additionally, boundary layer build-up on scroll side walls has a blocking effect in the scroll passage. Consequently, each vane will have different inlet conditions, such as the inlet mass flow and the inlet flow incidence.

The secondary flow in the scroll results from the non-equilibrium between the pressure and the centrifugal forces on the scroll side walls. Nonuniformities in the flow properties at the scroll inlet also result in secondary flow. This effect is similar to the secondary flow in cascade passages and pipe bends. The secondary flow consists mainly of vortices, whose strength varies along the scroll, causing a circumferential variation in the flow parameters. This factor again leads to different inlet flow conditions in each guide vane channel.

Additional vortices are created in the scroll passage due to the flow discharge to the guide vanes. Such vortices are similar to the corner vortices, but are not stationary. The depend on the geometry of the scroll and nozzle entrance arrangements. Therefore, these distributions add to the three dimensional flow behavior affecting the guide vane inlet flow properties.

A new analysis which describes the flow behavior in combined scroll-nozzle assembly of radial inflow turbines is reported by Hamed, et al. [1]. This analysis provides a better understanding of the mutual interaction effects of the flow in scroll-nozzle assembly. In a different but parallel investigation, Hamed, et al. [2] are presenting the solution for nonviscous rotational three dimensional scroll flow which determines the velocity components in the scroll cross sectional planes. Very few experimental measurements of scroll flow can be found in the literature. Reference [3] reports a detailed experimental and analytical study of the losses in both the vaned and vaneless regions of a radial inflow turbine nozzle.

In order to study the complicated flow behavior in a scroll-nozzle assembly, an experimental program has been undertaken in the Department of Aerospace Engineering and Applied Mechanics at the University of Cincinnati. As a first step in this program, experimental measurements of the through flow velocities in this scroll have been completed and reported in reference [4]. From this data, conclusions were drawn concerning the secondary flow behavior. This information was beneficial in the planning

of the current procedures for the measurement of secondary flows in the scroll.

RESEARCH SCROLL FACILITY

The test facility was designed to incorporate a complete radial inflow turbine scroll for testing using cold air. The most recent phase of experimental investigation was concerned with the measurement of the through flow and secondary flow velocities at different scroll cross sections. It is hoped that with this data a better understanding of the scroll flow behavior will be obtained. The scroll used was a nonsymmetric circular type with stator nozzle annulus consisting of 13 untwisted vanes. The turbine rotor was modified in such a way that the blades were removed and only the rotor hub was used in its place.

The scroll was originally part of a six kilowat single shaft Brayton cycle space power system using a 0.1262 m (4.97 in.) radial inflow turbine. The design and fabrication details of the system are given in reference [5]. The cold performance evaluation of the radial inflow turbine is given in reference [6].

Figure 1 shows the schematic diagram of experimental set-up. High pressure air was supplied from four large storage tanks, the air passed through a remotely controlled pressure regulating valve, standard orifice meter, filter and a flow regulating valve before entering the settling chamber. The temperature of the air was measured in the settling chamber. The filter was used to

trap dust particles up to a nominal diameter of about three microns. This prolonged the operating life of the hot film sensor.

The air supply was regulated by the flow regulating valve to give an air mass flow of 0.453 kg/sec (1 lb/sec). The air mass flow was measured by a standard orifice meter. The air from the settling chamber was fed to the scroll inlet through a convergent duct. The duct was circular in shape and blended smoothly into the inlet of the scroll.

Experimental Investigation:

A schematic diagram of the scroll is shown in Fig. 2. In the flow analysis of such a scroll, it is more convenient to define two cylindrical coordinate systems. The machine coordinate system (R,ϕ,Z) is fixed frame of reference with its Z axis as the machine shaft axis of the impeller. For the machine axes, the $\phi = 0$ line is 90° from the scroll entrance face as shown in Fig. 3. This set condition will be used for the purpose of discussion of the results. For the convenience of handling the experimental data in a specific scroll cross section, it is necessary to define a local axes system (r,θ,X) which is attached to the center of any particular scroll cross section under investigation. In this system, the X-axis is zero in the plane of the cross-section and is normal to this plane. Note that in the machine coordinate systems, the tangential direction at the center of any section coincides with the X-axis on the scroll cross section (the so-called through flow velocity direction).

Scroll Geometry:

Since curvilinear flow channels with variable cross-sections offer no characteristic length, Reynolds number ($\bar{V}d/v$) alone based on the average velocity $\bar{V}$ of steady flow ceases to be a criterion of describing the flow, as it is used for straight pipe flow. However, a simple dimensional analysis carried out suggests that such flow can be geometrically and dynamically compared by defining two nondimensional numbers, namely: ($\rho Q/\mu d$) and R/d where Q is the volume flow rate. In this work the scroll inlet mass flow Reynolds number was defined as $\frac{4}{\pi}\left(\frac{\dot{m}}{\mu d}\right)$ and is equal to 2.607×10^5. Figure 3 shows three scroll section locations. The first cross section is at $\phi = 0°$, the second at $\phi = 71°$ and the third at $\phi = 139°$.

Instrumentation:

The air mass flow was measured using a standard orifice meter. The temperature of the air was measured in the settling chamber using a simple commercial dial type thermometer with a stem. No pressure measurements were made except at the orifice meter. The velocity measurements inside the scroll were made using the TSI model 1213-20 hot film slant sensor shown in Figure 4. The cylindrical sensor element is 0.0508 mm (0.002 in.) in diameter, 1.016 mm (0.040 in.) long, and is at a slant angle of 45°. It is coated with alumina and gold plated at the ends where it is fixed to the prongs. The prongs are 12.7 mm (0.5 in.) long.

Probe Mount and Flow Measurement:

The positions of three scroll cross sections where the measurements have been taken are shown in Fig. 3. At each section, specially designed probe ports were welded at discrete angular locations, which allowed the probes to survey the complete scroll cross section. These ports were designed to mate properly with an automatic traversing mechanism. The probe was then mounted onto the electrically driven traversing mechanism. This permitted continuous movement of the probe into the cross section along radial (r) lines in order to minimize experimentation time and human errors. The rate of transverse could also be varied. The depth position of the probe was read on a graduated scale mounted on the traversing mechanism.

Figures 5a, 5b and 5c give the details of probe port locations for three cross sections. Figure 6 shows the relative po itions of the three scroll sections with respect to the machine axis. The radius of curvature R from the center of the scroll section makes an angle ε to the scroll horizontal. A table attached to the figure shows the radii of curvature and the corresponding ε of the three sections.

Procedure:

The high pressure air supply from air storage tanks was regulated to a pressure of 4.1368×10^5 N/m^2 gauge (60 psig) at the orifice meter using a pressure regulating valve. The air supply was passed through an air filter to a settling chamber where the temperature was measured. The pressure drop across the

orifice meter was varied with the flow regulating valve to give an actual air mass flow of 0.453 kg/sec (1 lb/sec). The air temperature did not vary appreciably from the nominal temperature of 21.11°C (70°F).

The flow velocity measurements inside the scroll were made using a hot film slant sensor. It was advantageous to use this sensor for three dimensional flow measurements since it required only one channel of electronic circuitry, when compared to two or three for cross wire probes. This consequently minimized measurement errors. Also, the obstruction to the flow field was reduced. The operation, calibration and the evaluation of velocities from the anemometer output signals are explained in Appendix A.

RESULTS AND DISCUSSION

The scroll inlet velocity measurements were made at two port locations. The results are shown in Fig. 7 and Table 1. The total velocity vector at every point of measurement in the scroll cross sections was resolved into three components. The through flow component, V_x, and the two secondary flow components V_h and V_v. Figures 8a, 8b and 8c show the measured through flow velocities in each of the three sections. The contour lines of the through flow velocity were obtained by normalizing the local measured velocities with respect to the scroll inlet average velocity of 16.36 m/sec (53.7 ft/sec). For all the measurements the mass flow rate was maintained at 0.453 kg/sec (1 lb/sec).

TABLE 1

THE SCROLL INLET VELOCITY DISTRIBUTION

Angular Position ϕ (deg)	Radial Depth r_d (cm)	Through Flow Velocity V_x (m/sec)
0	1.27	15.54
0	1.9	15.77
0	3.17	16.27
0	4.44	16.25
0	5.71	16.49
0	6.98	16.86
0	8.25	17.25
0	9.52	16.28
0	10.08	16.38
90	1.27	14.9
90	1.9	15.82
90	3.17	16.43
90	5.39	16.45
90	7.62	16.86
90	8.89	17.2
90	10.16	17.25

The through flow velocity contours are similar to the ones obtained using an x-probe given in reference [4]. The numerical values of the flow velocity components at various locations in the scroll are given in Appendix B.

Figure 9 shows the secondary flow velocity vectors at various points in scroll section 1. There are two secondary flow currents observable in this data which are schematically shown in Fig. 10. The horizontal components of the secondary flow velocity vectors are plotted and shown in Fig. 11. Inspection of this figure clearly illustrates the parting position of the secondary flow currents. The secondary flow pattern for scroll section 2 is shown in Fig. 12. Once again there are two secondary flow loops as illustrated in Fig. 13. However, the flow parting position has rotated in the clockwise direction. Moreover, the magnitude of the secondary velocities have increased. The horizontal components of the secondary flow velocity vectors for section 2 are shown in Fig. 14. The secondary flow pattern for scroll section 3 is shown in Figs. 15 through 17. Once again there are two recirculating zones and the flow parting position has rotated clockwise though not as much as that of the second section. The secondary flow currents observed during these tests are a result, in part, from a nonequilibrium between pressure and centrifugal forces. This imbalance, due to the nozzle discharge and the passage's curvature is directly related to the scroll geometry. For a better understanding of such phenomenon further testings are

necessary for scroll having different design configurations. Presently we are measuring the secondary and through flows in vaneless scroll and the results will be reported in separate report.

REFERENCES

1. Hamed, A., Baskharone, E. and Tabakoff, W., "A Flow Study in Radial Inflow Turbine Scroll-Nozzle Assembly," ASME Journal of Fluids Engineering, March 1978, Vol. 100, pp. 31-36.

2. Hamed, A., Abdallah, S. and Tabakoff, W., "Flow Study in the Cross Sectional Planes of a Turbine Scroll," AIAA Paper No. 77-714, AIAA 10th Fluid and Plasma Dynamics Conference, Albuquerque, New Mexico, June 27-29, 1977.

3. Khalil, I.M., Tabakoff, W. and Hamed, A., "Losses in Radial Inflow Turbines," ASME Journal of Fluids Engineering, September 1976, Vol. 98, pp. 364-373.

4. Tabakoff, W., Sheoran, Y. and Kroll, K., "Flow Measurements in a Turbine Scroll," Journal of Fluids Engineering, Vol. 102, September 1980, pp. 290-296.

5. Anon, "Design and Fabrication of the Brayton Cycle High Performance Turbine Research Package," Report APS-5281-R, AiResearch Mfg. Co. of Arizona, (NASA CR-72478), 1968.

6. Nusbaum, W.J. and Kofskey, M.G., "Cold Performance Evaluation of 4.97 inch Radial Inflow Turbine Designed for Single Shaft Brayton Cycle Space Power System," NASA TND 5090, 1969.

7. Schmidt, D.P. and Okishi, T.H., "Multistage Axial-Flow Turbomachine Wake Production, Transport and Interaction," Iowa State University No. ISU-ERI-AMES-77130, November 1976.

8. Thermo Systems Inc., "Instruction Manual for Model 1125 Calibrator."

Nomenclature

d	diameter of the scroll cross section, m
m_c, m_b	angular increments to yaw angles, deg., (eqs. 9 and 10, Appendix A)
$\dot{m}$	mass flow rate, kg/sec
Q	volume flow rate, m^3/sec
r	radius of the scroll cross section, m
r_d	radial depth of the measuring point, cm
R	radius of curvature of the machine coordinate system (fig. 2)
$\bar{S}$	the sensor axis (fig. 18)
$\bar{V}$	flow velocity vector, m/sec
V_h	horizontal component of the secondary flow velocity, m/sec
V_s	secondary flow velocity, m/sec
V_v	vertical component of secondary flow velocity, m/sec
V_x	through flow component of velocity, m/sec
x	x-axis of probe coordinate system (fig. 18)
X	X-axis of scroll coordinate system (fig. 2)
y	y-axis of probe coordinate system (fig. 18)
z	z-axis of probe coordinate system (fig. 18)
Z	Z-axis of scroll coordinate system (fig. 2)
α	sensor yaw angle, deg. (fig. 18)
ε	angle between the radius of curvature and the horizontal axis, deg. (fig. 6)
θ	angular position of the measuring parts, deg. (fig. 5)
θ_o	angle between sensors axis and x-axis, deg. (fig. 18)

θ_p probe pitch angle, deg. (fig. 18)

θ_y probe yaw angle, deg. (fig. 18)

μ dynamic viscosity, kg/m sec

ρ density, kg/m^3

ϕ scroll angular coordinate, deg.

APPENDIX A

HOT FILM VELOCITY MEASUREMENT TECHNIQUE

A schematic diagram of the probe along with coordinate axes used is shown in Fig. 18. The z coordinate is along the axis of the probe and x coordinate is located in such a way that the sensor lies in the x-z plane. The sensor axis $\bar{S}$ makes an angle θ_o with the x axis and α is the angle between the sensor axis and the flow velocity vector $\bar{V}$. The direction of the velocity vector with respect to the probe is defined by θ_y, the probe yaw angle and θ_p, the probe pitch angle. A relationship among the various angles is given by the equation:

$$\cos\alpha = \cos\theta_o \cos\theta_p \cos\theta_y + \sin\theta_o \sin\theta_p \qquad (1)$$

A detailed description of the measurement procedure is given in reference [7].

Usually sensors are calibrated with flow normal to the sensor, i.e. sensor yaw angle $\alpha = 90°$. If a flow measurement is taken at a sensor angle other than 90°, in this case, the effective velocity V_e indicated by the sensor will be different from the actual flow velocity V. Schmidt and Okishi [7] used a second order emprical correlation to express the relationship between these two velocities as follows:

$$\frac{V_e}{V} = b_0 + b_1\alpha + b_2\theta_p + b_3V + b_4\alpha^2 + b_5\theta_p^2 + b_6V^2 + b_7\alpha\theta_p + b_8\alpha V + b_9\theta_p V \qquad (2)$$

The coefficients b_0 through b_9 were determined using the calibration procedure given below.

Calibration Procedure:

In order to obtain the coefficients for the above equation, the probe was calibrated with the help of TSI Model 1125 calibrator [8] which uses a calibration nozzle. A probe fixture was developed to vary the yaw and pitch angles of the probe with respect to the flow from the nozzle. Initially the probe was calibrated for flow normal to the sensor ($\alpha = 90°$) and the relationship between signal output and velocity was curve fitted using a polynomial curve fit. Using the probe fixture, the sensor was swept through various ranges of yaw and pitch angles. An example of a typical set of angular increments is shown in Table 2. The measurements shown in the table are only for one particular flow velocity. However, the calibration was carried out over the entire velocity vector envelope which was to be encountered in the experiment. The flow at the exit of the calibration nozzle was at about 21.11°C (70°F) and at atmospheric pressure. The air temperature in the scroll during measurements did not vary much from this temperature. Hence, no temperature correction was applied. However, since the air pressure was different, density corrections were applied to all the sensor output readings.

TABLE 2

VELOCITY = 76.19 m/sec (250 ft/sec)

θ_p Pitch Angle Deg.	θ_y YAW Angle Deg.	Signal Output Volts	θ_p Pitch Angle Deg.	θ_y YAW Angle Deg.	Signal Output Volts
-6	50	7.283	+3	50	7.216
	40	7.19		40	7.111
	30	7.121		30	6.87
	20	6.899		20	6.737
	10	6.813		10	6.606
	0	6.702		0	6.508
	-10	6.716		-10	6.529
	-20	6.875		-20	6.619
	-30	7.044		-30	6.737
	-40	7.136		-40	6.893
	-50	7.222		-50	7.113
-3	50	7.273	+6	50	7.191
	40	7.184		40	7.04
	30	7.073		30	6.817
	20	6.828		20	6.680
	10	6.743		10	6.535
	0	6.642		0	6.434
	-10	6.657		-10	6.467
	-20	6.757		-20	6.545
	-30	6.953		-30	6.686
	-40	7.093		-40	6.838
	-50	7.192		-50	7.063
0	50	7.247			
	40	7.145			
	30	6.96			
	20	6.782			
	10	6.675			
	0	6.579			
	-10	6.590			
	-20	6.687			
	-30	6.807			
	-40	7.002			
	-50	7.160			

A computer program was developed to obtain the coefficients necessary for the equation (2), from a least square curve fit of effective velocity calibration data obtained for different probe orientations and air speeds. Two sets of coefficients were obtained. One for the velocity data at positive yaw angles and the other for the negative yaw angles.

Operation:

The magnitude and direction of the velocity in the scroll at any one point was determined by taking the measurements at three probe angle orientations and reducing the data using equations (1) and (2). Referring to Fig.19, if the three probe orientations are A, B and C, the resulting six equations are:

For position A,

$$\frac{V_{e,a}}{V} = b_{0a} + b_{1a}\,\alpha_a + b_{2a}\,\theta_p + b_{3a}\,V + b_{4a}\,\alpha_a^2 + b_{5a}\,\theta_p^2 + b_{6a}\,V^2 + b_{7a}\,\alpha_a\theta_p + b_{8a}\,\alpha_a V + b_{9a}\,\theta_p V \tag{3}$$

$$\cos\alpha_a = \cos\theta_o \cos\theta_p \cos\theta_y + \sin\theta_o \sin\theta_p \tag{4}$$

For position B,

$$\frac{V_{e,b}}{V} = b_{0b} + b_{1b}\,\alpha_b + b_{2b}\,\theta_p + b_{3b}\,V + b_{4b}\,\alpha_b^2 + b_{5b}\,\theta_p^2 + b_{6b}\,V^2 + b_{7b}\,\alpha_b\theta_p + b_{8b}\,\alpha_b V + b_{9b}\,\theta_p V \tag{5}$$

$$\cos\alpha_b = \cos\theta_o \cos\theta_p \cos\theta_{yb} + \sin\theta_o \sin\theta_p \qquad (6)$$

For position C,

$$\frac{V_{e,c}}{V} = b_{0c} + b_{1c}\,\alpha_c + b_{2c}\,\theta_p + b_{3c}\,V + b_{4c}\,\alpha_c^2 + b_{5c}\,\theta_p^2 + b_{6c}\,V^2 + b_{7c}\,\alpha_c\theta_p + b_{8c}\,\alpha_c\,V + b_{9c}\,\theta_p V \qquad (7)$$

$$\cos\alpha_c = \cos\theta_0 \cos\theta_p \cos\theta_{yc} + \sin\theta_o \sin\theta_p \qquad (8)$$

Since the last two probe orientations are made by fixed angular increments with respect to the first,

$$\theta_{yb} = \theta_y + m_b \qquad (9)$$

$$\theta_{yc} = \theta_y - m_c \qquad (10)$$

The coefficients b_0 through b_9 in the equations (3) to (8) were known. The three effective velocities $V_{e,a}$, $V_{e,b}$ and $V_{e,c}$ being measured values, the above six equations could be solved simultaneously for the 6 unknown variables α_a, α_b, α_c, θ_p, V, and θ_y. A computer code has been developed to solve the above equations simultaneously using the Newton-Raphson numerical method. With V, θ_p and θ_y determined, the velocity vector, $\bar{V}$ is completely specified with respect to the probe coordinate system. The velocity vector was then resolved into three components in the scroll coordinate system (horizontal velocity, through vector and vertical velocity).

The three probe measurement angles θ_y, θ_{yb} and θ_{yc} were so chosen that they lie in regions of high sensor sensitivity. To avoid probe prong interference, the shorter prong was always positioned into the flow upstream of the longer prong. First, the probe was rotated so as to face the flow direction, which is characteristically given by a minimum voltage output signal. The probe was then turned by 5° in the positive direction to get position A (Fig. 19) and the signal recorded. Position B was obtained by turning the probe by 30° in the positive direction and the reading taken. Finally the third reading was taken by rotating the probe in the negative direction by 30° from position A to obtain position C.

APPENDIX B

SCROLL SECTION 1

Radial Depth (cm) Y_d	Through Flow Velocity (m/sec) V_x	Secondary Flow Velocity (m/sec)		
		Vertical Component V_v	Horizontal Component V_h	Resultant V_s
		Angular Position θ = -3°		
0.63	15.84	-3.96	-1.12	4.11
1.90	17.51	-3.07	-1.20	3.30
3.17	19.30	-1.15	-1.31	1.74
3.81	19.30	-1.15	-1.31	1.74
4.44	19.30	-1.15	-1.31	1.74
5.71	18.50	-2.20	-0.97	2.40
6.98	18.41	-2.30	-0.90	2.46
8.25	17.99	-2.98	-0.62	3.04
9.52	17.74	-3.52	0.42	3.55
		Angular Position θ = 20°		
0.63	13.18	-4.27	3.27	5.37
1.90	16.01	-4.42	-0.28	4.43
3.17	19.34	-1.41	-1.78	2.27
3.81	19.58	-1.44	-1.80	2.30
4.44	20.02	-1.39	-1.54	2.08
5.71	20.84	-1.02	-1.96	2.21
6.98	21.07	-1.15	-1.51	1.90
8.25	21.23	-1.60	-1.13	1.96
9.52	21.18	-2.10	-0.44	2.15
		Angular Position θ = 45°		
1.90	15.64	-1.01	2.63	2.82
3.17	17.18	-0.32	2.53	2.55
3.81	18.82	0.51	1.66	1.75
4.44	18.55	0.09	2.16	2.16
5.71	19.83	0.36	1.98	2.01
6.98	19.42	-0.10	3.84	3.84
8.25	24.84	2.16	-1.04	2.40
9.52	23.92	2.71	1.81	3.26

SCROLL SECTION 1

Radial Depth (cm) Y_d	Through Flow Velocity (m/sec) V_x	Secondary Flow Velocity (m/sec)		
		Vertical Component V_v	Horizontal Component V_h	Resultant V_s
		Angular Position θ = 67.5°		
1.90	14.57	-0.34	3.16	3.18
3.17	14.22	-0.27	4.95	4.96
3.81	14.62	-0.28	5.23	5.24
4.44	18.53	1.04	1.48	1.81
5.71	18.06	0.48	3.79	3.82
6.98	21.72	0.92	0.94	1.31
8.25	22.35	0.33	2.10	2.13
9.52	24.55	-0.43	1.51	1.56
		Angular Position θ = 90°		
1.90	13.36	1.15	4.33	4.48
3.17	14.22	1.64	4.68	4.96
3.81	16.62	0.96	2.59	2.77
4.44	17.79	1.09	1.81	2.12
5.71	19.29	1.35	1.59	2.09
6.98	21.45	1.24	1.31	1.81
8.25	22.77	1.78	2.27	2.88
9.52	24.49	2.20	2.99	3.71
		Angular Position θ = 112.5°		
1.90	15.15	1.51	2.04	2.54
3.17	16.13	1.66	2.23	2.78
3.81	16.64	1.73	2.33	2.90
4.44	18.00	1.31	1.32	1.86
5.71	19.38	1.89	1.42	2.36
6.98	20.57	2.03	1.54	2.55
8.25	21.73	6.13	0.03	6.13
9.52	22.97	7.47	0.15	7.47
		Angular Position θ = 135°		
0.63	12.10	6.39	0.85	6.45
1.90	15.71	3.77	-0.59	3.82
3.17	17.13	3.89	-1.03	4.02
4.44	18.73	3.65	-2.31	4.32
5.71	17.86	5.40	-0.38	5.41
6.98	19.48	5.73	-1.86	6.02
8.25	21.01	5.74	-2.24	6.16
9.52	21.33	6.94	-2.28	7.31

SCROLL SECTION 2

Radial Depth (cm) Y_d	Through Flow Velocity (m/sec) V_x	Secondary Flow Velocity (m/sec)		
		Vertical Component V_v	Horizontal Component V_h	Resultant V_s
		Angular Position θ = -3°		
1.27	9.34	-9.99	5.29	11.31
1.90	19.51	-2.22	1.75	2.83
3.17	20.27	-1.88	1.29	2.28
3.81	20.73	-1.30	1.50	1.99
4.44	19.89	-2.26	1.57	2.75
5.71	20.10	-2.31	1.81	2.93
6.98	20.27	-2.54	2.53	3.59
8.25	20.57	-2.38	2.08	3.16
		Angular Position θ = 19°		
1.27	19.34	-0.18	2.61	2.62
1.90	17.93	-1.61	3.29	3.67
2.54	18.42	-1.41	3.03	3.34
3.17	18.99	-0.76	3.14	3.23
3.81	20.12	0.15	2.80	2.81
4.44	19.69	-0.55	3.50	3.54
5.08	19.98	-0.34	3.57	3.58
5.71	19.98	-0.31	4.40	4.41
6.35	19.88	-0.46	4.59	4.61
6.98	21.83	-1.19	4.30	4.46
7.62	21.09	-0.52	4.89	4.91
8.25	21.19	-0.41	5.12	5.13
		Angular Position θ = 41°		
1.90	16.32	-1.44	1.97	2.44
3.17	18.48	-0.47	0.31	0.57
3.81	18.44	1.12	2.69	2.91
4.44	18.47	0.97	3.14	3.29
5.71	18.69	0.63	4.22	4.26
6.98	19.47	0.80	4.57	4.64
8.25	21.23	2.48	4.49	5.13

SCROLL SECTION 2

Radial Depth (cm) Y_d	Through Flow Velocity (m/sec) V_x	Secondary Flow Velocity		
		Vertical Component V_v	Horizontal Component V_h	Resultant V_s
		Angular Position θ = 65°		
1.27	14.24	3.63	5.44	6.54
1.90	15.63	3.65	4.90	6.11
2.54	16.15	3.71	4.81	6.08
3.17	17.00	4.20	4.59	6.22
3.81	18.03	4.69	4.22	6.31
4.44	18.82	5.43	4.06	6.78
5.08	18.71	5.08	5.13	7.22
5.71	19.85	5.25	4.68	7.03
6.35	20.31	5.68	5.35	7.80
6.98	18.87	5.57	7.56	9.39
7.62	21.73	6.43	5.23	8.29
8.25	22.51	6.47	5.70	8.63
		Angular Position θ = 87.5°		
1.27	15.60	2.91	2.62	3.92
1.90	16.27	2.71	2.48	3.68
3.17	17.62	3.08	2.25	3.82
3.81	17.62	3.27	3.42	4.73
4.44	18.56	3.55	2.97	4.63
5.71	20.16	3.88	3.30	5.09
6.98	21.60	4.42	3.57	5.68
8.25	24.79	4.68	2.48	5.30
		Angular Position θ = 134°		
1.75	15.67	6.56	-2.75	7.11
2.38	15.14	7.34	-1.87	7.58
3.02	18.02	5.89	-4.55	7.44
3.65	17.21	6.81	-3.27	7.55
4.29	18.23	6.88	-4.44	8.18
5.56	19.60	7.24	-4.65	8.60
6.83	19.81	8.67	-4.64	9.83
8.10	20.72	9.78	-5.45	11.20

SCROLL SECTION 3

Radial Depth (cm) Y_d	Through Flow Velocity (m/sec) V_x	Secondary Flow Velocity (m/sec)		
		Vertical Component V_v	Horizontal Component V_h	Resultant V_s
		Angular Position θ = -1°		
1.27	19.35	-2.44	3.90	4.60
1.90	19.63	-2.24	3.57	4.21
2.54	19.83	-2.02	3.69	4.21
3.81	19.80	-2.25	4.05	4.63
4.44	19.56	-2.44	4.15	4.81
5.08	19.50	-2.65	4.42	5.15
5.71	18.51	-3.86	4.75	6.12
6.35	20.57	-2.00	4.75	5.16
		Angular Position θ = 19°		
1.27	17.24	-2.03	3.20	3.79
1.90	17.82	-1.65	2.44	2.95
3.17	18.96	-0.80	2.53	2.65
3.81	19.30	-0.73	2.77	2.87
4.44	20.57	0.35	2.26	2.28
5.08	19.22	-1.39	3.81	4.05
5.71	20.27	-0.41	3.47	3.50
6.35	20.55	-0.68	3.54	3.60
		Angular Position θ = 41°		
1.27	15.78	0.05	5.67	5.67
1.90	18.10	0.77	4.21	4.28
2.54	18.28	1.31	4.48	4.67
3.17	16.87	0.01	6.15	6.15
3.81	18.26	0.49	5.40	5.42
4.44	18.27	0.35	6.03	6.04
5.08	20.85	2.44	4.39	5.02
5.71	20.68	2.33	5.24	5.74
6.35	21.63	3.16	4.72	5.68
		Angular Position θ = 63°		
0.63	15.18	2.03	5.76	6.11
1.27	16.56	1.67	4.18	4.50
1.90	17.25	1.87	3.81	4.25
2.54	17.96	1.73	3.60	3.99
3.17	19.29	2.52	2.90	3.84
3.81	20.15	2.76	2.65	3.83
4.44	20.41	3.06	3.29	4.50
5.08	20.63	3.31	3.38	4.73
5.71	21.27	3.19	3.44	4.69
6.35	23.61	4.04	1.80	4.42

SCROLL SECTION 3

Radial Depth (cm) Y_d	Through Flow Velocity (m/sec) V_x	Secondary Flow Velocity (m/sec)		
		Vertical Component V_v	Horizontal Component V_h	Resultant V_s
		Angular Position θ = 88°		
1.27	15.91	3.12	3.26	4.51
1.90	16.82	3.11	2.51	4.00
2.54	17.62	2.92	3.04	4.21
3.17	17.42	3.23	4.18	5.28
3.81	18.11	6.57	3.49	7.44
4.44	17.61	7.27	4.79	8.70
5.08	18.82	7.63	4.79	9.01
5.71	18.87	8.23	5.64	9.98
6.35	20.69	8.86	5.07	10.20
		Angular Position θ = 110°		
1.27	14.93	6.61	1.85	6.86
1.90	15.72	6.78	1.58	6.96
2.54	17.56	6.09	0.57	6.11
3.17	18.46	6.17	0.46	6.19
3.81	18.82	7.01	0.70	7.04
4.44	18.91	7.91	1.23	8.00
5.08	18.94	8.90	1.75	9.07
5.71	21.75	8.31	-0.54	8.33
6.35	20.42	10.04	2.14	10.27
		Angular Position θ = 133°		
1.27	13.90	8.06	-2.14	8.34
1.90	15.21	8.17	-3.35	8.83
2.54	15.86	8.29	-3.19	8.88
3.17	16.29	8.53	-3.54	9.24
3.81	15.41	9.86	-2.95	10.29
4.44	17.31	9.39	-4.04	10.22
5.08	18.68	8.37	-1.87	8.57
5.71	19.46	8.38	-2.25	8.68
6.35	20.80	8.41	-3.30	9.04

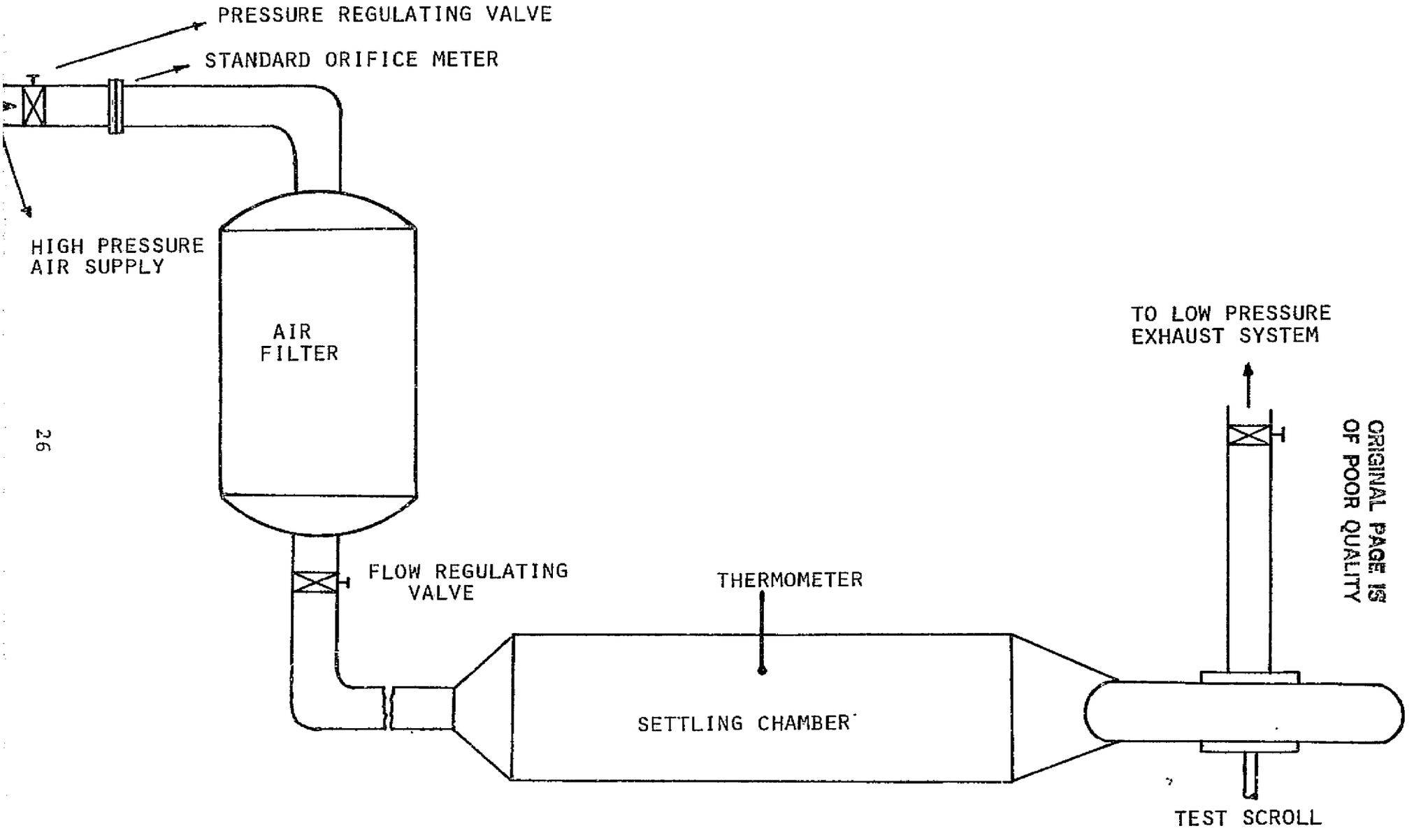

FIG. 1 . SCHEMATIC DIAGRAM OF THE EXPERIMENTAL SET-UP.

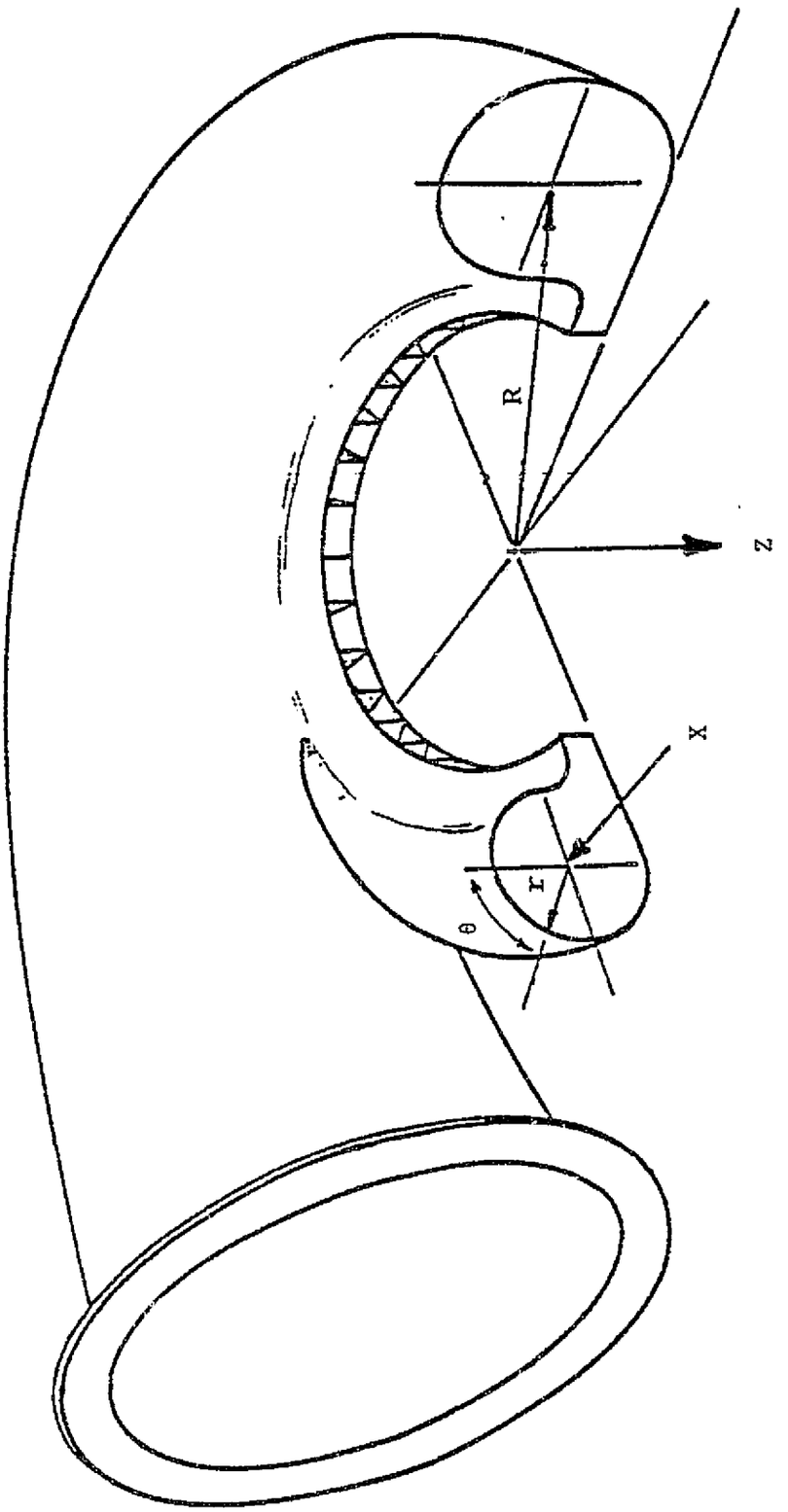

FIG. 2. SCROLL SCHEMATIC DIAGRAM.

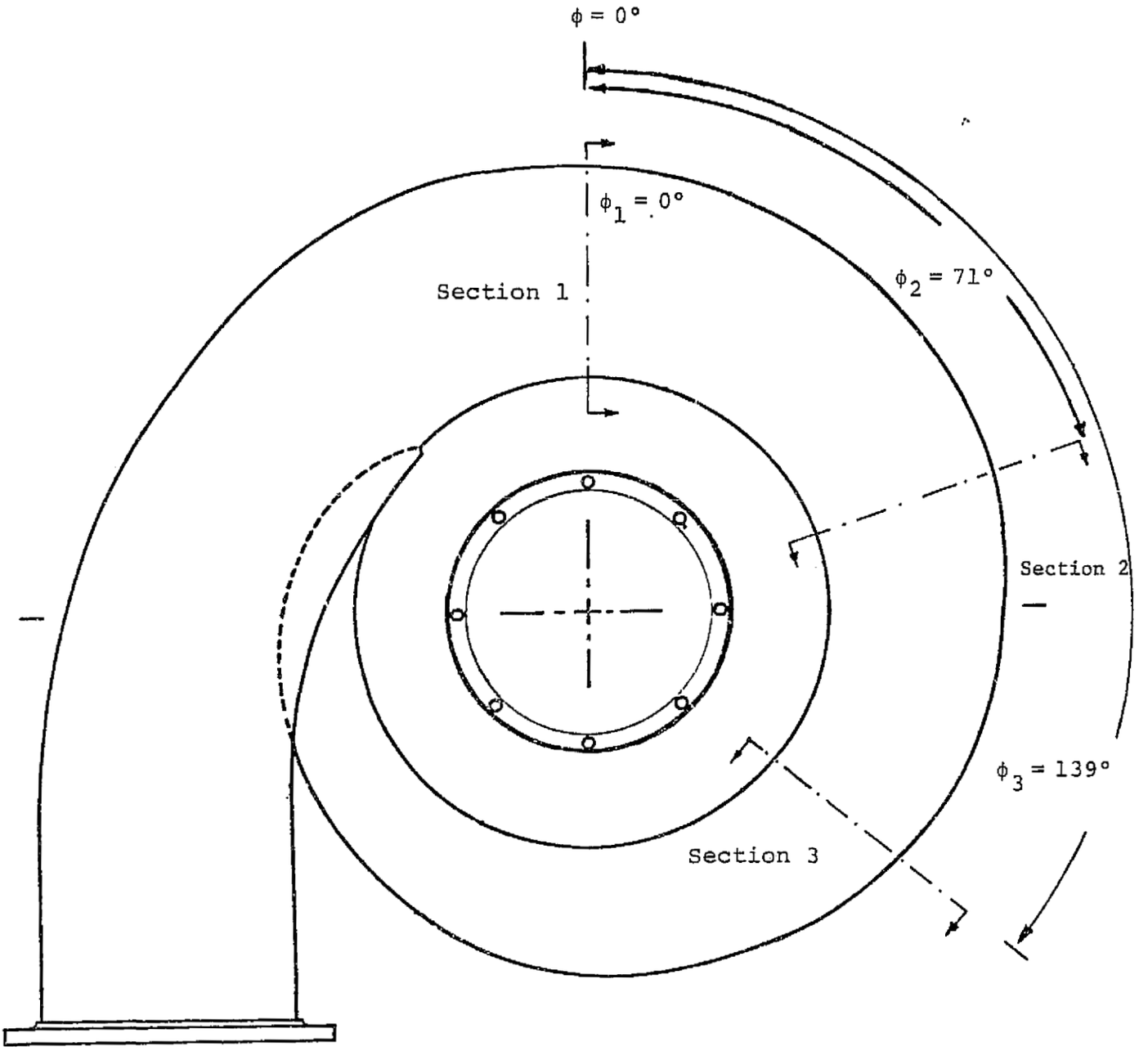

FIG. 3. PLAN VIEW OF THE SCROLL

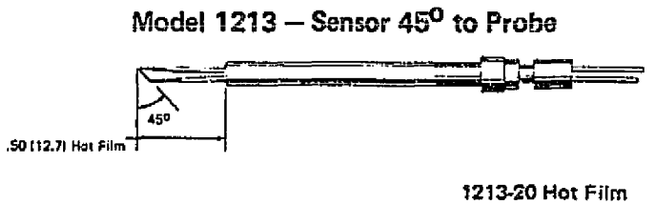

FIG. 4. SCHEMATIC DIAGRAM OF HOT FILM SENSOR.

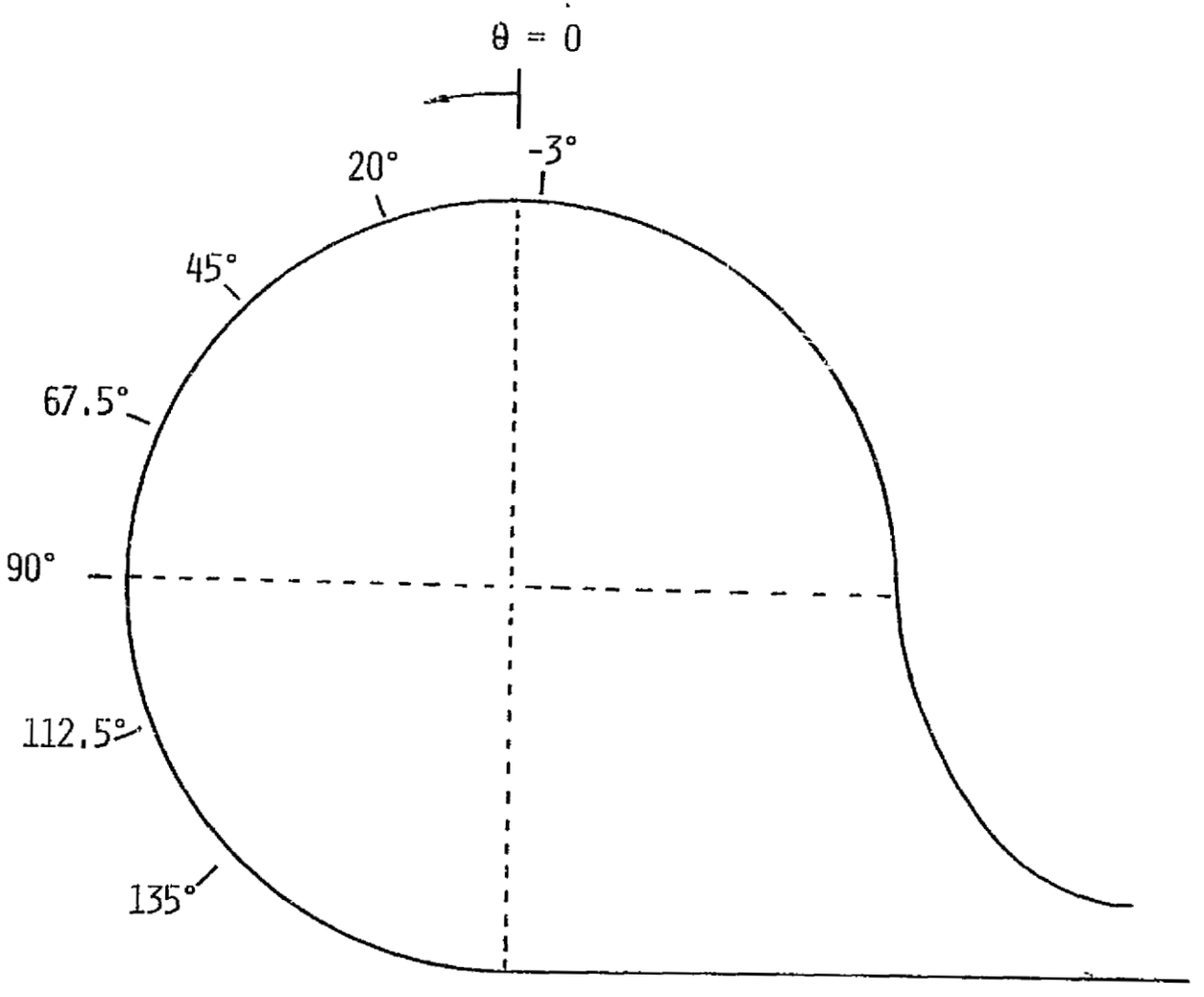

FIG. 5A. ANGULAR POSITION OF PROBE PORTS (SECTION 1).

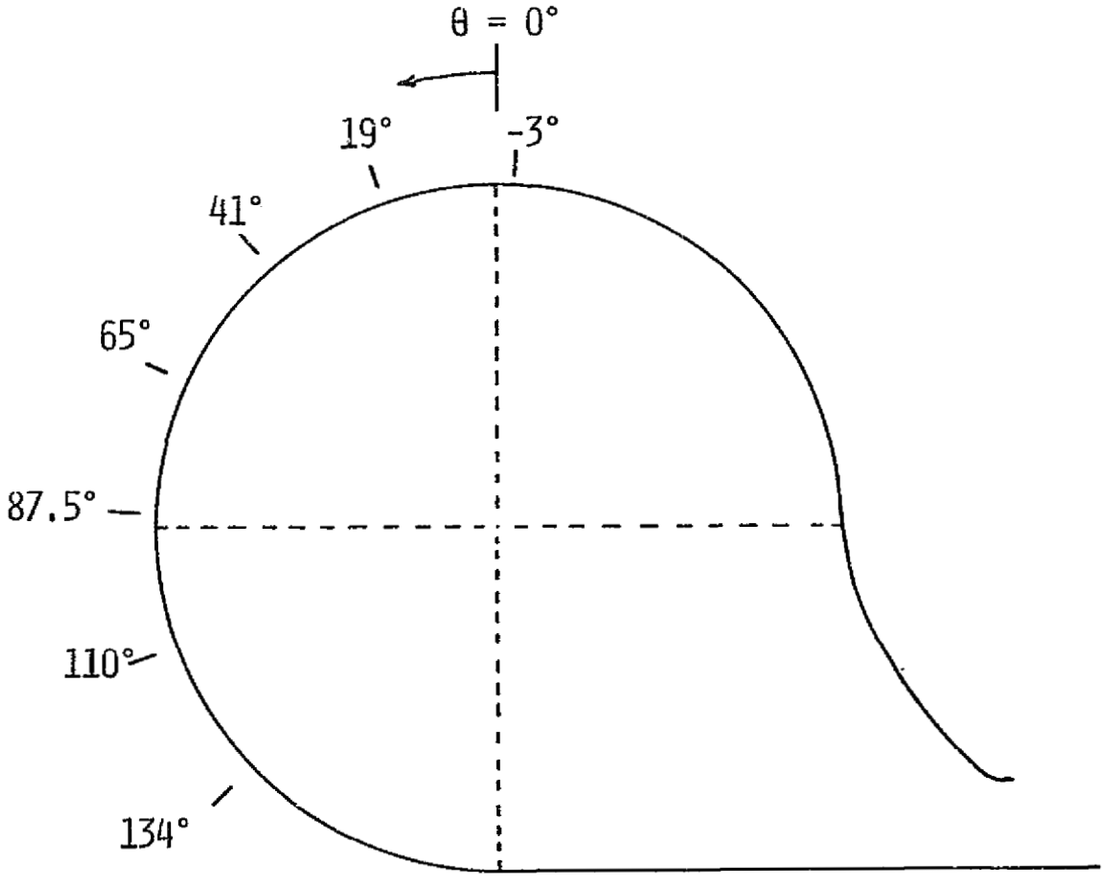

FIG. 5B. ANGULAR POSITION OF PROBE PORTS (SECTION 2).

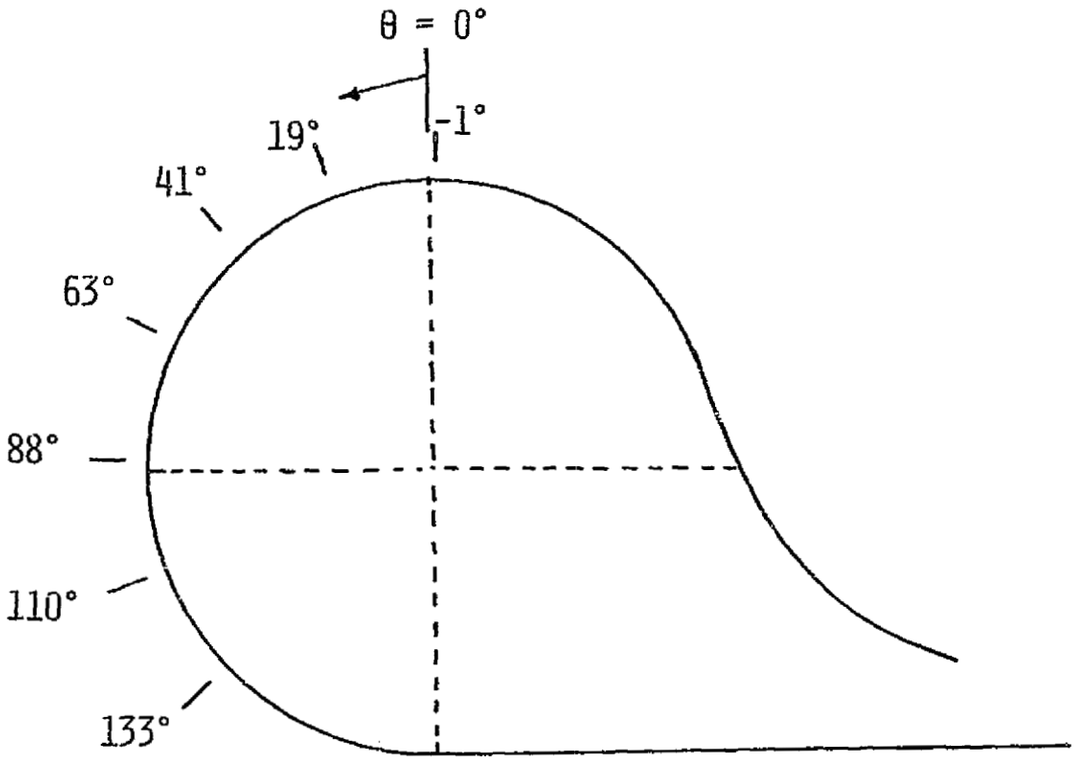

FIG. 5c. ANGULAR POSITION OF PROBE PORTS (SECTION 3).

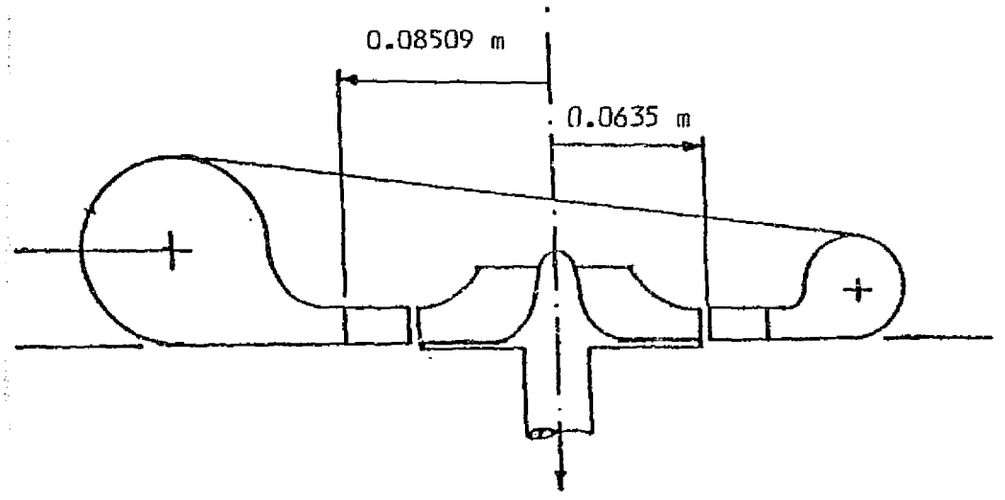

SECTION	R	r	ϵ
1	0.1821 m	0.05156 m	16.46 deg.
2	0.1756 m	0.04445 m	14.66 deg.
3	0.1692 m	0.036576 m	12.49 deg.

EXIT NOZZLE HEIGHT = 0.011 m

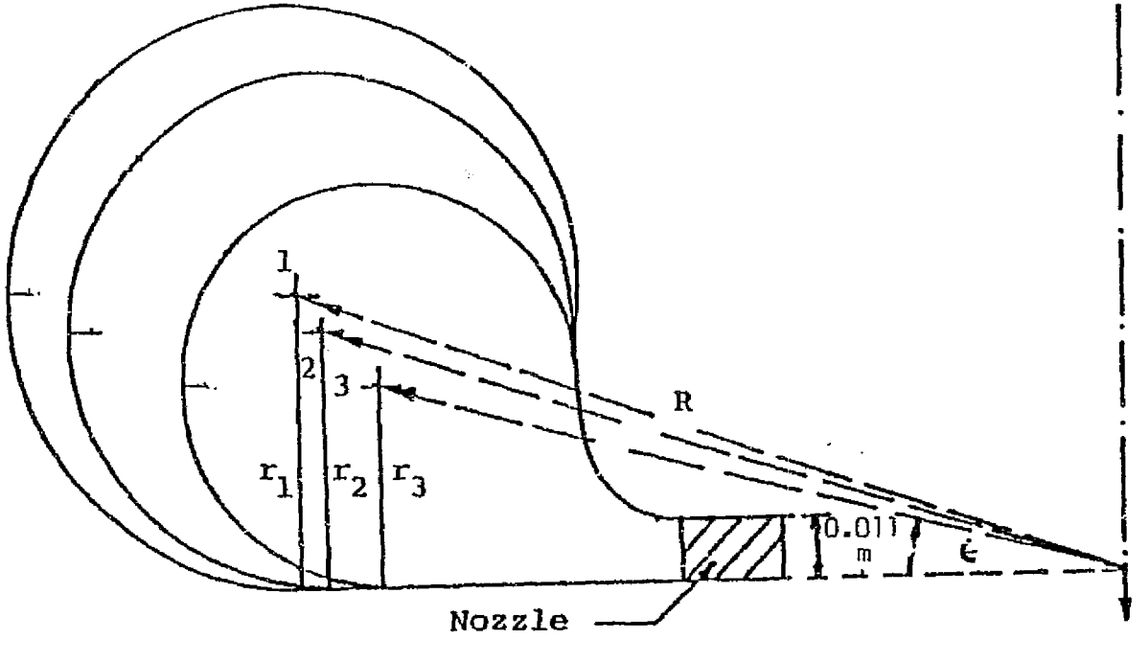

FIG. 6. RELATIVE POSITION OF THREE SECTIONS WITH RESPECT TO THE MACHINE AXIS.

FIG. 7. THE SCROLL INLET VELOCITY DISTRIBUTION (M/SEC).

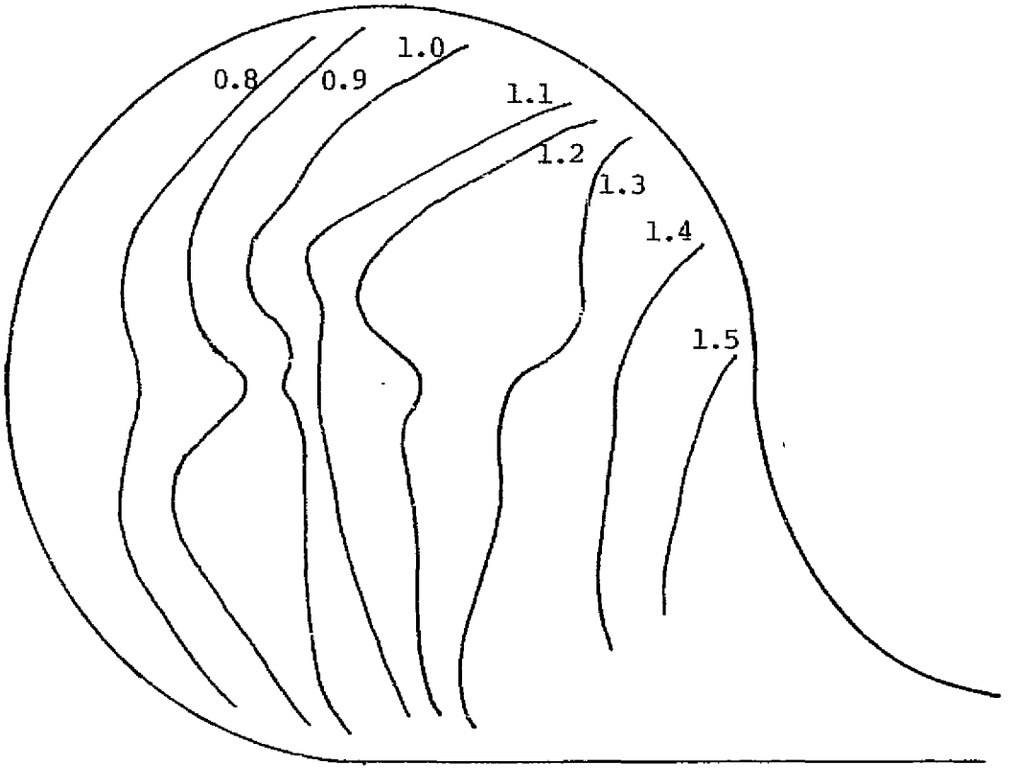

FIG. 8A. NORMALIZED THROUGH FLOW VELOCITY CONTOURS (SECTION 1).

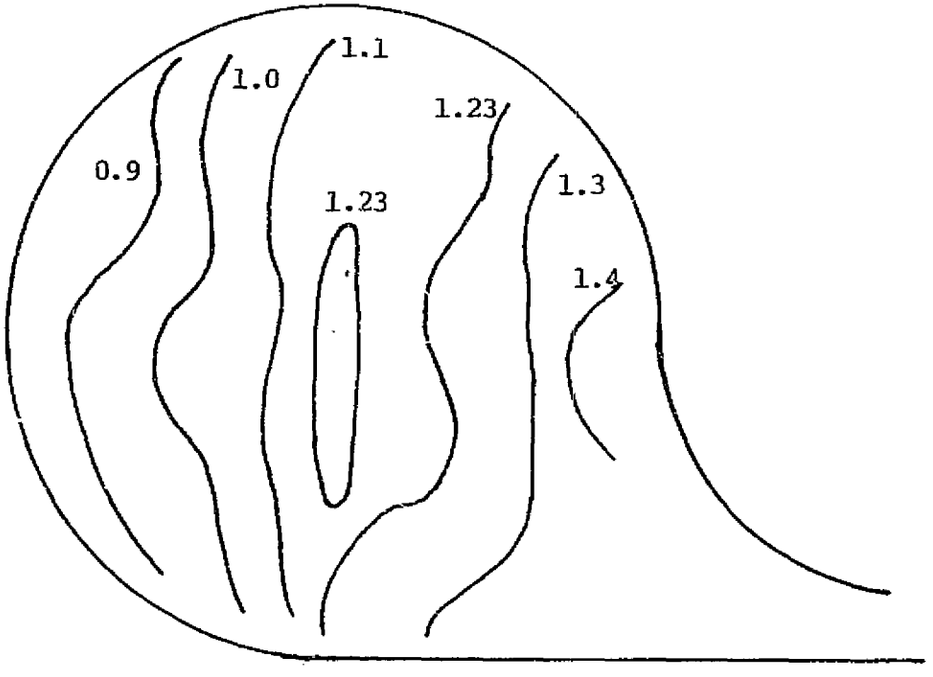

FIG. 3B. NORMALIZED THROUGH FLOW VELOCITY CONTOURS (SECTION 2)

FIG. 8C. NORMALIZED THROUGH FLOW VELOCITY CONTOURS (SECTION 3)

FIG. 9. SECONDARY FLOW VELOCITY VECTORS (SECTION 1).
(SCALE: 1 CM = 12 M/SEC)

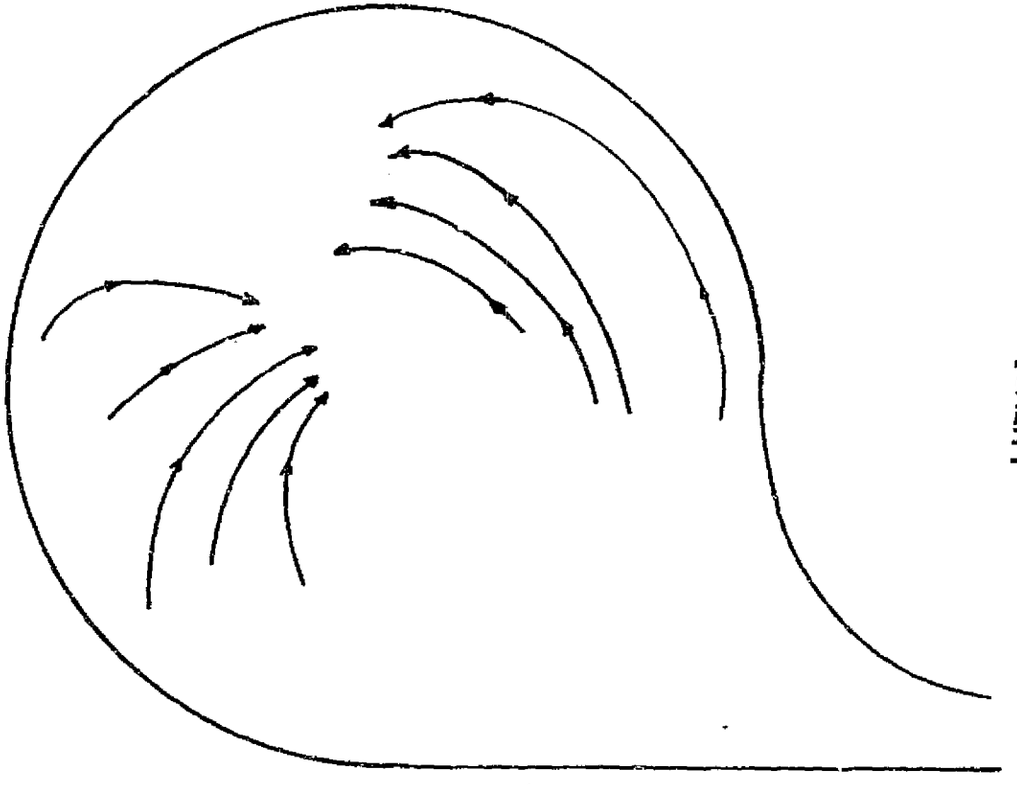

FIG. 10. SCHEMATIC DIAGRAM OF RECIRCULATION ZONES (SECTION 1).

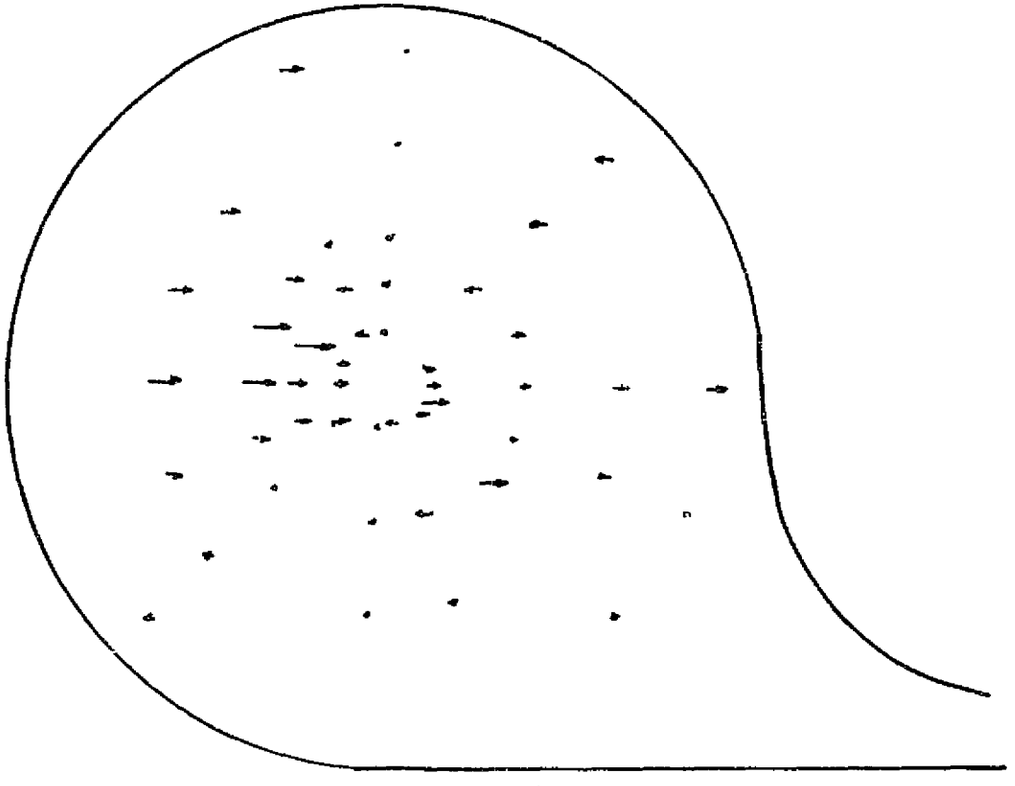

FIG. 11. HORIZONTAL COMPONENT OF SECONDARY FLOW VELOCITY VECTORS (SECTION 1)
(SCALE: 1 CM = 10 M/SEC)

FIG. 12. SECONDARY FLOW VELOCITY VECTORS (SECTION 2)
(SCALE: 1 CM = 12 M/SEC)

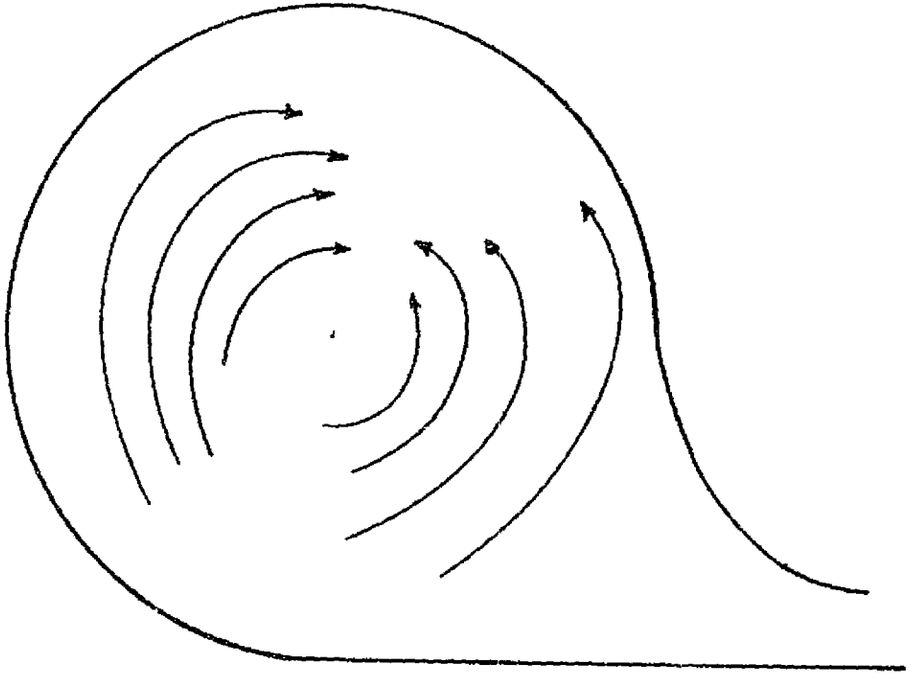

FIG. 13. SCHEMATIC DIAGRAM OF RECIRCULATION ZONES (SECTION 2).

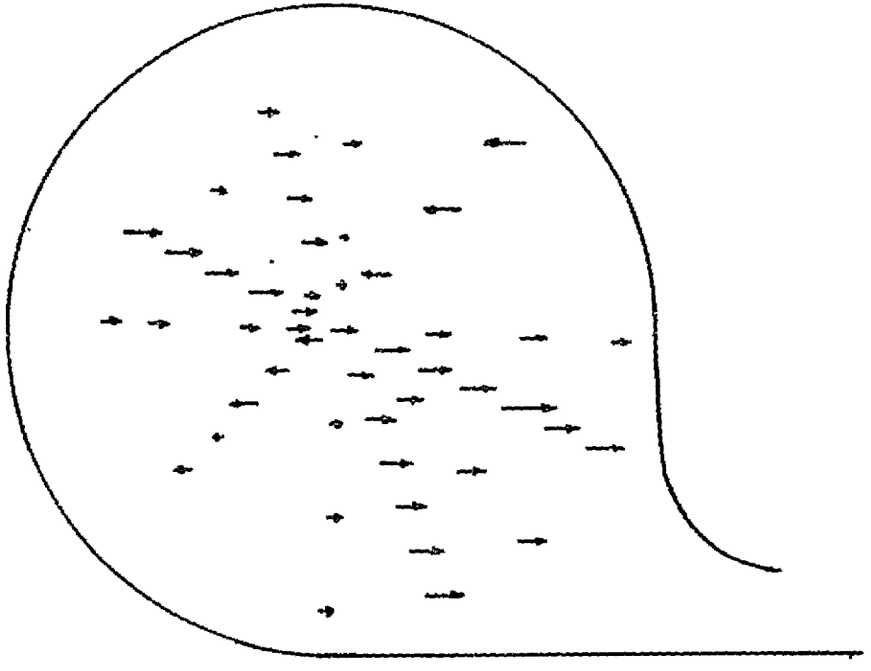

FIG. 14. HORIZONTAL COMPONENTS OF SECONDARY FLOW VELOCITY VECTORS, (SECTION 2) (SCALE: 1 CM = 10 M/SEC).

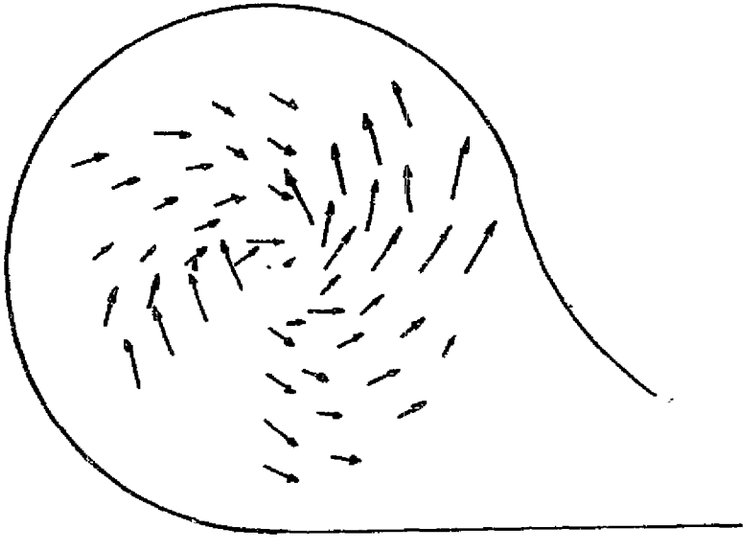

FIG. 15. SECONDARY FLOW VELOCITY VECTORS (SECTION 3)
(SCALE: 1 CM = 12 M/SEC)

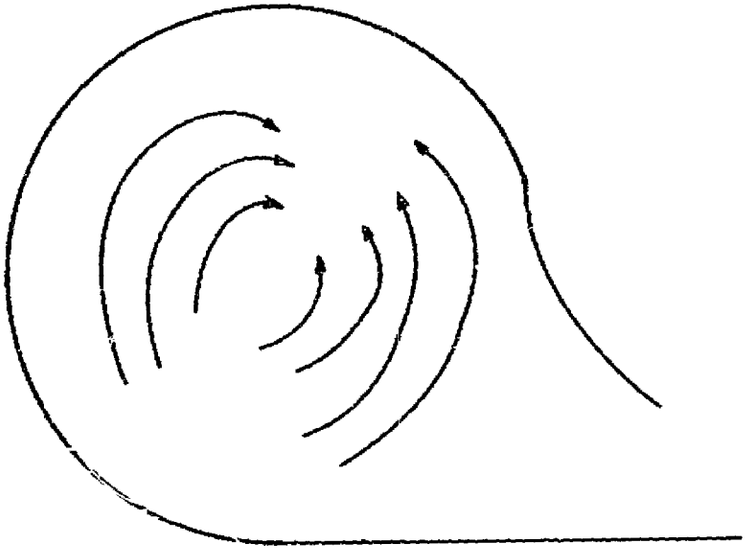

FIG. 16. SCHEMATIC DIAGRAM SHOWING RECIRCULATION ZONES (SECTION 3).

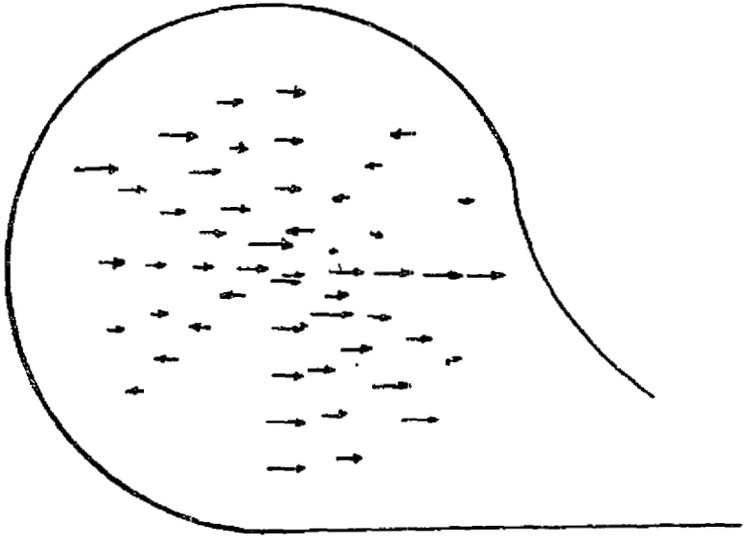

FIG. 17. HORIZONTAL COMPONENTS OF SECONDARY FLOW VELOCITY VECTORS (SECTION 3)
(SCALE: 1 CM = 10 M/SEC)

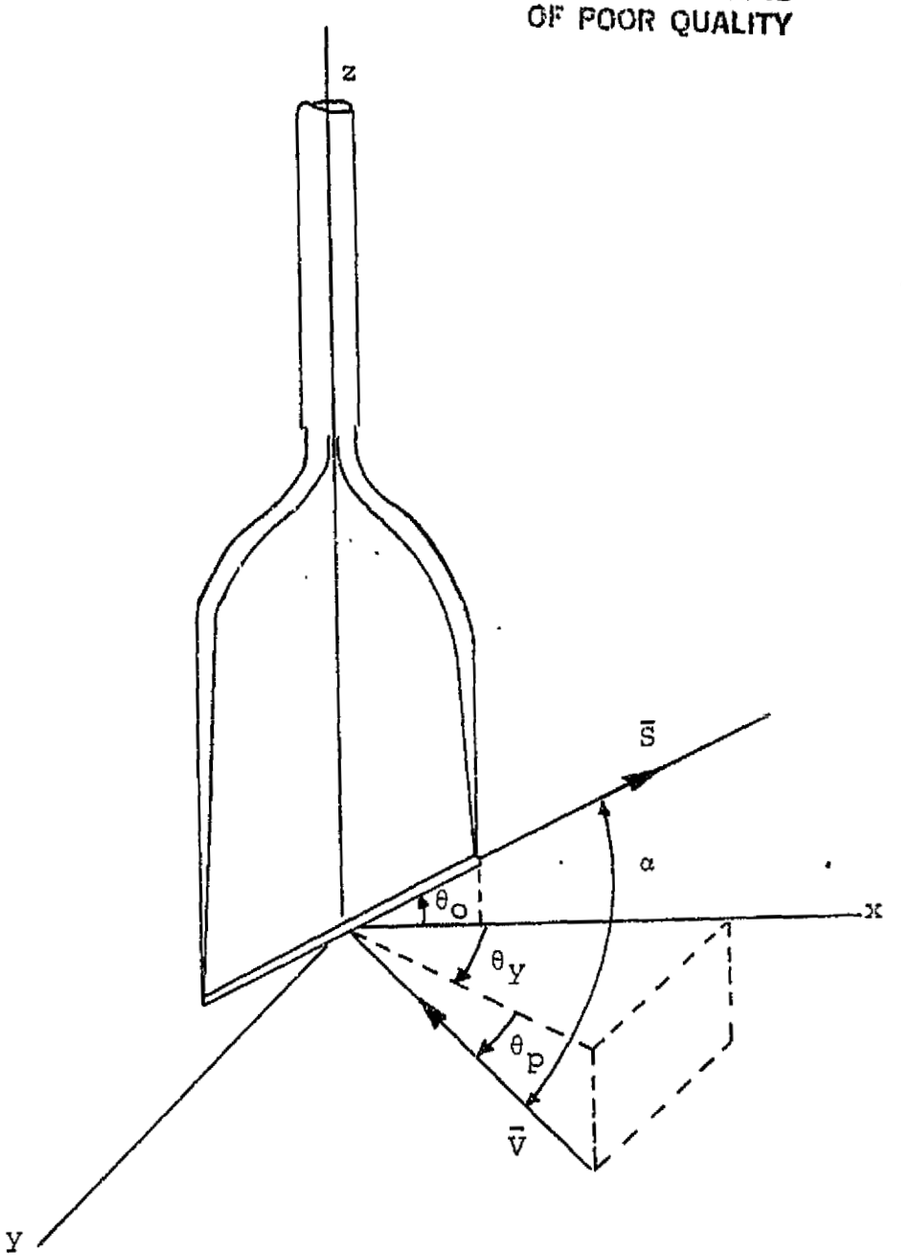

FIG. 18. PROBE COORDINATE AXES.

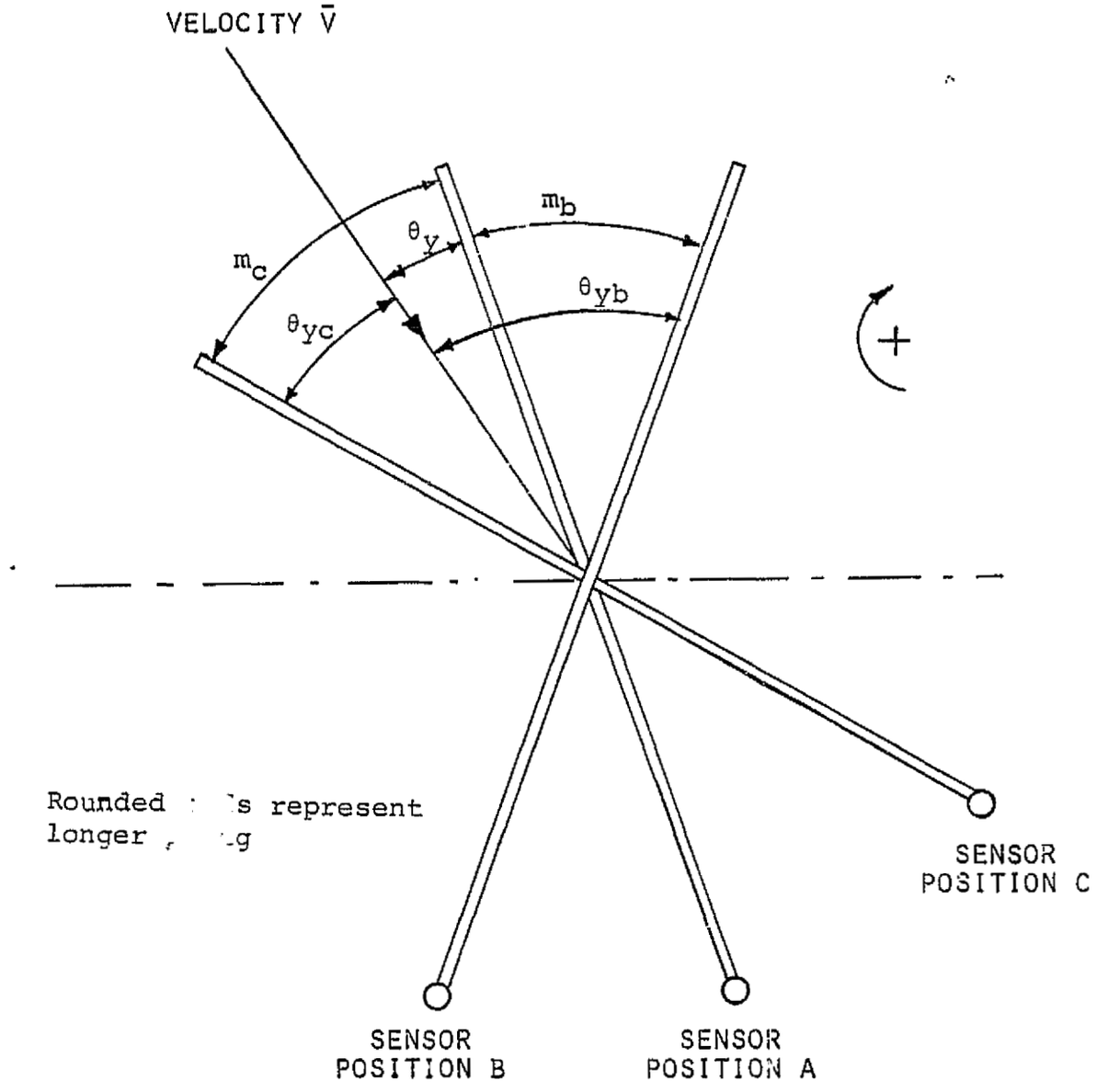

FIG. 19. PROBE MEASUREMENT POSITIONS AND NOMENCLATURE, VIEWED FROM ABOVE ALONG PROBE AXIS.